Design and analysis of highly sensitive solid core gold-coated hexagonal photonic crystal fiber sensor based on surface plasmon resonance

Monika Kiroriwal (k.kiroriwal@gmail.com)
Deenbandhu Chhotu Ram University of Science and Technology https://orcid.org/0000-0003-2777-4850

Poonam Singal
Deenbandhu Chhotu Ram University of Science and Technology

Research Article

Keywords: Photonic crystal fiber, detection, surface plasmon resonance, sensitivity, resolution

Posted Date: April 26th, 2021

DOI: https://doi.org/10.21203/rs.3.rs-389085/v1

Design and analysis of highly sensitive solid core gold-coated hexagonal photonic crystal fiber sensor based on surface plasmon resonance

Monika Kiroriwal[1] and Poonam Singal[2]

[1]Research Scholar, Electronics & Communication department, Deenbhandu Chottu Ram University of Science & Technology, Sonepat, India.

[2]Professor, Electronics & Communication department, Deenbhandu Chottu Ram University of Science & Technology, Sonepat, India.

Corressponding author: k.kiroriwal@gmail.com

Abstract

In this article, a surface plasmon-based hexagonal photonic crystal fiber sensor is numerically computed and studied. Metallic layer thickness and lattice period are optimized to 30 nm and 1.75 µm respectively to enhance the sensor performance. Sensor sensitivity is obtained by employing the finite element method by enclosing the structure with a perfectly matched layer. This studied sensor uncovers the wavelength sensitivity of 8000nm/RIU, amplitude sensitivity of 3959 /RIU, and minimum detection ability of $1.25x10^{-5}$ RIU for the analyte refractive index range from 1.36 to 1.40. The simulated results' variations are also analyzed by altering the metallic layer thickness, lattice period, and air hole diameter. The computed PCF sensor might be a promising aspirant in the area of chemical sensing, bio-molecule detection, and biological sample recognition.

Keywords

Photonic crystal fiber, detection, surface plasmon resonance, sensitivity, resolution

1. Introduction

Sensors are essential devices that detect the component amount of an estimation article and convert this amount into a readable signal, which is shown on an instrument. Furthermore, detecting technology is an innovation that utilizes sensors to gain data by sensing the physical, chemical, and biological properties and converting them into coherent signal. In recent years, optical sensing technique (OST) gained attention due to its numerous applications in the different aspects of science and technology from industry to real life.[1, 2]

In the present era, surface plasmon resonance (SPR) based optical fiber sensors have become the primary technique in OST.[3] Furthermore, SPR has been a savvy research subject for recent 20 years due to its accommodation in real-time sample detection, non-obtrusive, high affectability, and label-free handling.[4] Initial prism-based SPR sensor[5] and optical fiber-

based SPR sensor[6] had some limitations in terms of numerical aperture and complexity in fabrication. SPR sensors using photonic crystal fiber have been used to overcome these limitations, and become popular because of appealing properties, such as design flexibility, tunable dispersion and birefringence, tight light confinement, and single-mode function.[7] These SPR-PCF sensors are proving themselves as a suitable candidate in various areas like water testing, salinity testing, [8] gas, liquid, and drug detection, [9] food safety, [10] bio-chemical sample recognition, and blood component detection.[11]

Internal coating and external coating are two famous approaches for plasmonic material coating. In internal coating, metal is coated at the inner layer of the air hole.[12] Although, this approach provides high sensor performance but has two major drawbacks. First one is the uniform metal deposition, it is a difficult task during fabrication, and the second one is the analyte injection into the micron-sized air hole, it can limit the real-time application. [13] The external coating approach has been utilized to resolve these drawbacks, [14] where metal layer is circulated on the external boundary of the PCF. The sensing layer is in direct contact with plasmonic metal layer. Generally, detecting attributes of sensors rely upon the selection of plasmonic materials**.** Gold, copper, silver, and aluminum are a few plasmonic materials that have been used in the vast majority of the current works in the writing. [15-18]

M. B. Hossain et al. presented a hexagonal PCF biosensor utilized an external sensing approach. This silver coated PCF ensures the wavelength sensitivity of 21000 nm/RIU with amplitude sensitivity of 2456 /RIU. [19] M. N. Shakib et al. demonstrated a novel structure of PCF biosensor to acquire the wavelength sensitivity in value of 16000 nm/RIU and amplitude sensitivity of 780 RIU^{-1}. In this model, outer ring air holes are cut to make slots, which are difficult to fabricate. [20] A number of cores also affect the performance of the sensor. A double-core SPR-PCF sensor is designed and analyzed by M.N. Shakib et al.[21] It offers a wavelength sensitivity of 8000nm/RIU and a high value of amplitude sensitivity of 700 RIU^{-1} with a figure of Merit of 138 RIU^{-1}. A. Shafkat proposed a PCF sensor to display the wavelength sensitivity of 10,700 nm/RIU with a suitable amplitude sensitivity of 1770 RIU^{-1}. This gold-coated duplex-core model has fewer air holes of different diameters, which increases the fabrication complexity.[22] A. A. Rifat et al. illustrated a PCF plasmonic biosensor and achieved a high sensor resolution with high sensitivities of 4000 nm/RIU and 478 RIU^{-1} .[23] S. Akter et al. demonstrated an open channel-based PCF sensor to achieve a wavelength

sensitivity of 5000nm/RIU and amplitude sensitivity of 396 $RIU^{-1}$for near to visible wavelength range.[24] S. Chakma et al. displayed a gold-deposited PCF-SPR biosensor and presents a wavelength sensitivity of 9000 nm/RIU and high resolution with amplitude sensitivity of 318 RIU^{-1} .[25] Md. R. Hasan et al. demonstrated a spiral shape PCF to provide an amplitude sensitivity of 420.4 RIU^{-1} and wavelength sensitivity of 4300 nm/RIU for vertical-polarized mode.[26]

All SPR-PCF sensors discussed above have some restrictions for fabrication due to complex geometry. Proposed sensor provides a comparatively high sensitivity over a large range of refractive index detection (1.36 to 1.40) as shown in Table 1 and also offers a simple geometry in terms of fabrication. PCF sensor design and modeling is elaborated in second section. Optimized sensor performance and effects of design parameters on sensitivity is analyzed in third section followed by conclusion.

2. Sensor design and numerical modeling

Fig. 1 displays the transverse representation of an investigated gold-coated PCF sensor. All the circular air holes ($d = 1.2\,\mu m$) are patterned in a hexagonal manner in the presented sensor geometry. Gold, a well-known metal material, is circulated on the PCF's outer surface. Gold is an inactive and less oxidized material.[27] One small-size air hole is inserted in the centre, and one air hole from the second layer is omitted to make a solid core for light confinement. Three air holes near the solid core are kept small to reduce the air gap between the metal and core area. This arrangement is suitable to generate Surface Plasmon's (SPs). Optimized design parameters are achieved by varying the lattice period Λ=1.75 µm, small air hole diameter d_s =0.4 µm, and plasmonic metal thickness T_g . A 1.5 µm thick perfectly matched layer (PML) is employed as a final circulation for minimizing the unavoidable leakage from the cladding part of the PCF.[28] Due to simple structure of proposed sensor, this can be manufactured by conventional stack and draw technique,[29] and chemical vapor deposition method is suitable for making a gold metal layer with thickness of $T_g = 30nm$.[27] Conventional silica is selected as a host material to get the high-performance sensor.

The dielectric constant is used to get the complex refractive index of gold. Drude-Lorentz equation is practiced to determine this constant value as given in[27] as:

$$\varepsilon_{Gold} = \varepsilon_{\infty} - \frac{\omega_d^2}{\omega(\omega + j\gamma_d)} - \frac{\Delta\varepsilon\Omega_L^2}{(\omega^2 - \Omega_L^2) + j\Gamma_L\omega} \quad (1)$$

Where ε_{Gold} is gold permittivity, $\varepsilon_{\infty} = 5.9673$is high-frequency permittivity, $\omega_d = 2113.6 \times 2\pi$ THz is plasma frequency, and $\gamma_d = 15.92 \times 2\pi$ THz denotes decaying frequency. Angular frequency $\omega = 2\pi c/\lambda$ at working wavelength λ, here c is constant light velocity, has a value of 3x10^8 m/sec, and weighting factor $\Delta\varepsilon = 1.09$. Moreover, $\Omega_L = 650.07 \times 2\pi$ THz is oscillator strength and Lorentz's spectral width is referred as $\Gamma_L = 104.86 \times 2\pi$ THz.[20] Sellmier equation is defined for silica's refractive index as below:

$$n^2(\lambda) = 1 + \frac{D_1\lambda^2}{\lambda^2 - E_1} + \frac{D_2\lambda^2}{\lambda^2 - E_2} + \frac{D_3\lambda^2}{\lambda^2 - E_3} \quad (2)$$

Here, Sellmier coefficients are D1=0.69616300, D2=0.407942600, D3=0.897479400, E1=0.00467914826, E2=0.0135120631, and E3=97.9340025.[11]

The analyte layer with a thickness of 1.2 µm is deposited on the metal layer's outer surface to sense the molecules efficiently. Analyte refractive index (n_a) is taken from 1.36 to 1.40. The whole sensor structure is structured and simulated using software COMSOL Multi-physics. The Finite element method is employed to get the desired simulated results under the finer mesh mapping.

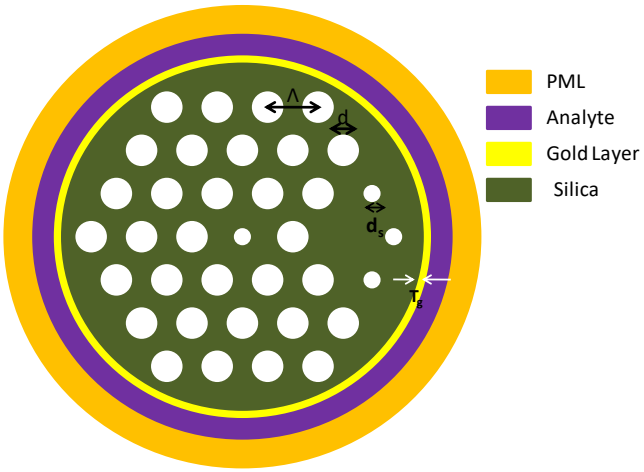

Fig. 1 transverse image of SPR-PCF sensor

3. Sensor performance based on simulated results

The investigated SPR sensor works on dynamics of the interaction point of a solid core-clad zone of propagated light that is episode on the dielectric metal part and emits free electrons. The confined real core mode index and the surface plasmon (SP) mode index are equivalent to each other at a particular wavelength, and generate surface plasmon wave (SPW).[30]

Each sensor performance is discussed by calculating the confinement loss, which is expressed as given formula:[26]

$$\alpha(dB/cm) = 8.686 \times \frac{2\pi}{\lambda} \times \mathrm{Im}(n_{eff}) \times 10^4 \qquad (3)$$

Where, Im(n_{eff}) is an imaginary part of the confined mode refractive index. Analyte refractive index (ARI) has a great impact on the confined mode index (n_{eff}). An unknown sensing medium can be identified by observing the shift of resonant peaks towards higher wavelengths.

The confined electric fields for x-polarized, initial resonance and SP modes are illustrated in Fig. 2 (a)-(c). The dispersion relation is shown in Fig. 3 for core and SP-guided mode. Dash black line and dash red line describe the real effective index for x-confined mode and SPP mode, respectively. At 680 nm, due to phase-matching condition, real effective refractive index of x-confined ode and SP polariton mode are intersect with each other, and a sharp

peak occurs in the confinement loss curve (solid blue line). This peak is a clear indication of power transfer from fiber guided core-mode to surface plasmon mode, and that specific wavelength is assumed as resonance wavelength (RW). The peak value of confinement loss 110.89 dB/cm is acquired at a resonance wavelength of 680 nm for the ARI of 1.38.

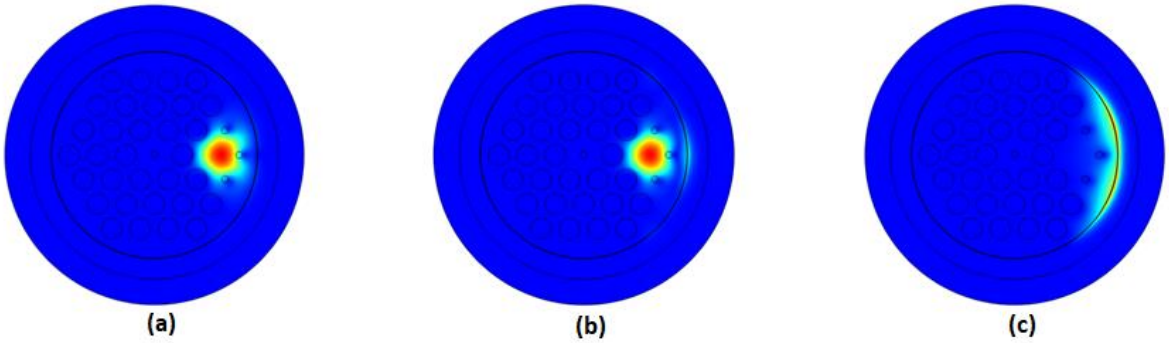

Fig. 2 Power distribution mode (a) X-polarized mode (b) Resonance mode (c) Surface Plasmon mode

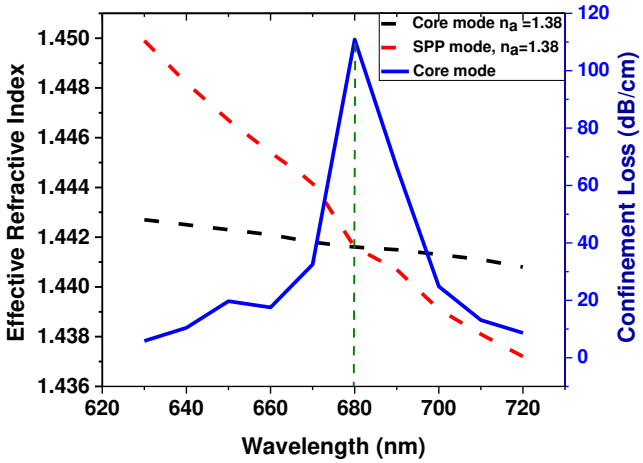

Fig. 3 Intersection of Core and SPP mode with core confinement loss curve

3.1 Sensor performance for different value of n_a (Analyte refractive index)

Confinement loss (CL) is the first factor which has a profound impact on sensor performance. This CL changes with the analyte refractive index value. From Fig. 4(a), it is clear when there is a change in analyte RI (ARI) from 1.36 to 1.40 with a gap of 0.01; then peak is shifted from a smaller wavelength to longer wavelength as follows. ARI changes from 1.36 to 1.37, peak is shifted from 620 to 640 nm, from 1.37 to 1.38 peak is changed from

640 to 680 nm, from 1.38 to 1.39 peak is shifted from 680 to 740 nm, from 1.39 to 1.40 peak is changed from 740 to 820 nm, respectively. The peak value of confinement loss varies from 49.89 to 230.1 dB/cm for the ARI range from 1.36 to 1.40. Based on these different CL values, wavelength sensitivity (WS) is calculated using wavelength interrogation method (WI) defined by.[22]

$$S_w(nm/RIU) = \Delta\lambda_P / \Delta n_a \quad (4)$$

Here $\Delta\lambda_P$ represents the wavelength difference between two adjacent peaks and Δn_a is the difference between two adjacent ARIs. In this paper, it has a fix value of 0.01. The proposed sensor geometry shows $\Delta\lambda_P$ as a variation of 20, 40, 60, and 80 nm with respect to the Δn_a variation from 1.36 to 1.40 with a gap of 0.01. Therefore, according to the eq. (4), the numerically computed WSs are 2000, 4000, 6000, and 8000 nm/RIU, correspondingly and plotted in Fig. 4(b). Wavelength resolution is also an essential factor to measure the sensing ability of the sensor for a minimum variation in the ARI as characterized in the literature:[24]

$$WR(RIU) = \Delta n_a \times \Delta\lambda_{\min} / \Delta\lambda_P \quad (5)$$

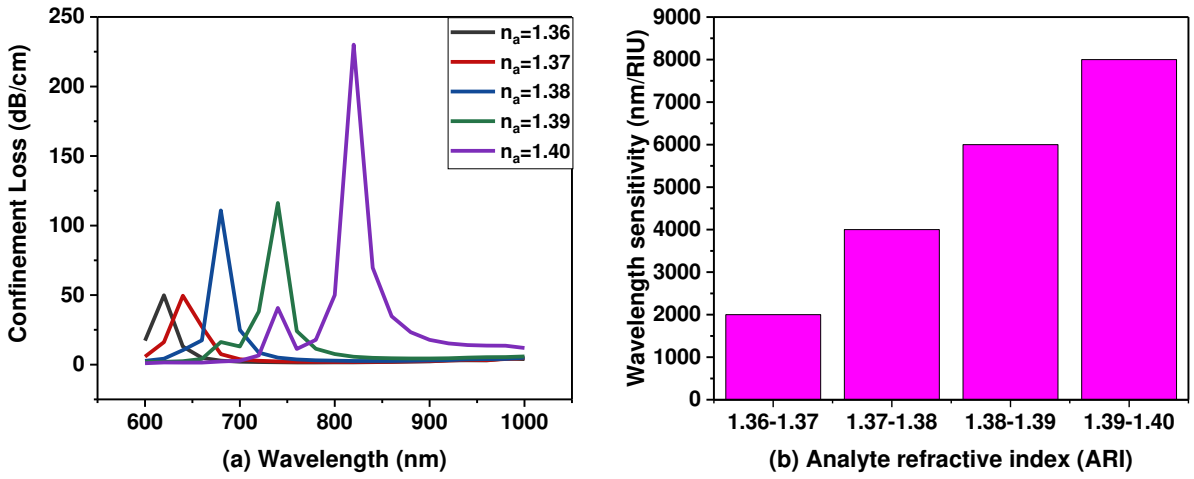

Fig. 4 Simulated curves of confinement loss when Λ=1.75 µm, d= 1.2, d_s =0.4 µm, and T_g=30 nm for different values of ARI from 1.36 to 1.40 (b) Wavelength sensitivity chart for different ARI

Maximum WR of the reported PCF sensor is observed about 1.25x10^{-5} RIU for a maximum resonance wavelength difference of 80 nm while assuming $\Delta\lambda_{\min} = 0.01$ nm. So, this sensing device can sense the deviation in the ARI in 10^{-5} order. WI technique is little difficult to measure the sensor performance. To overcome this limitation, amplitude interrogation

method (AIM) is utilized to calculate the sensitivity in terms of amplitude at a specific wavelength.[31] Given expression explains the amplitude sensitivity (AS) in eq. (6).

$$S_A(1/RIU) = -\left(\frac{1}{\alpha(\lambda, n_a)}\right)\left(\frac{d\alpha(\lambda, n_a)}{\Delta n_a}\right) \quad (6)$$

Where $\alpha(\lambda, n_a)$ displays the CL and $d\alpha(\lambda, n_a)$ signify the CL difference. Amplitude sensitivity is determined and plotted in Fig. 5 with respect to the wavelength. The highest amplitude sensitivity of 3959 RIU^{-1} is acquired at 820 nm wavelength with a n_a value of 1.39.

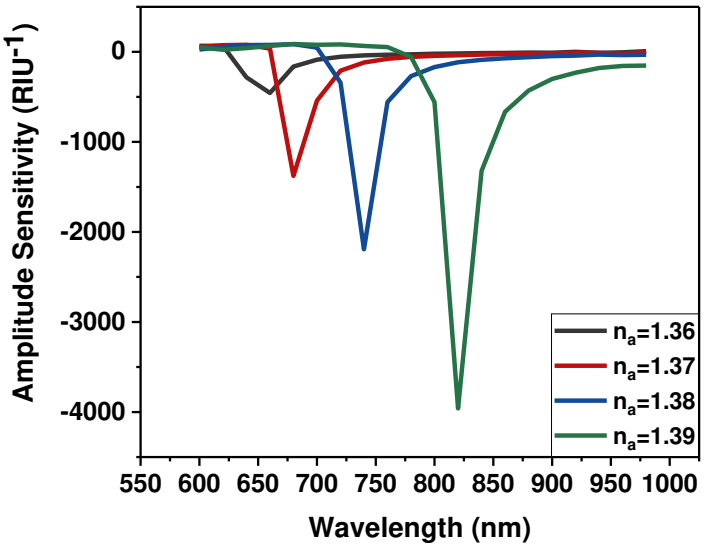

Fig. 5 Dependence of amplitude sensitivity according to the range of ARI from 1.36 to 1.39

3.2 Sensor performance analysis on the effect of gold layer thickness

The gold metallic layer has a significant influence on sensor sensitivity.[27] CL and amplitude sensitivity can be altered with the variation in metallic layer thickness T_g. Here, the CL spectra for ARI of 1.38 and 1.39 with the variation in T_g from 30 nm to 50 nm are illustrated in Fig. 6(a).

It is clear from Fig. 6(a), peak loss value is reduced by increasing the gold layer thickness. As per obtained CL values, amplitude sensitivity of 2191 for T_g =30 nm, 1548 for T_g =40 nm, and 826 $RIU^{-1}$for T_g =50 nm has been achieved for the ARI of 1.38 as displayed in Fig. 6(b).

Maximum AS accomplished for 30 nm gold layer thickness, so it is suitable for sensor performance analysis.

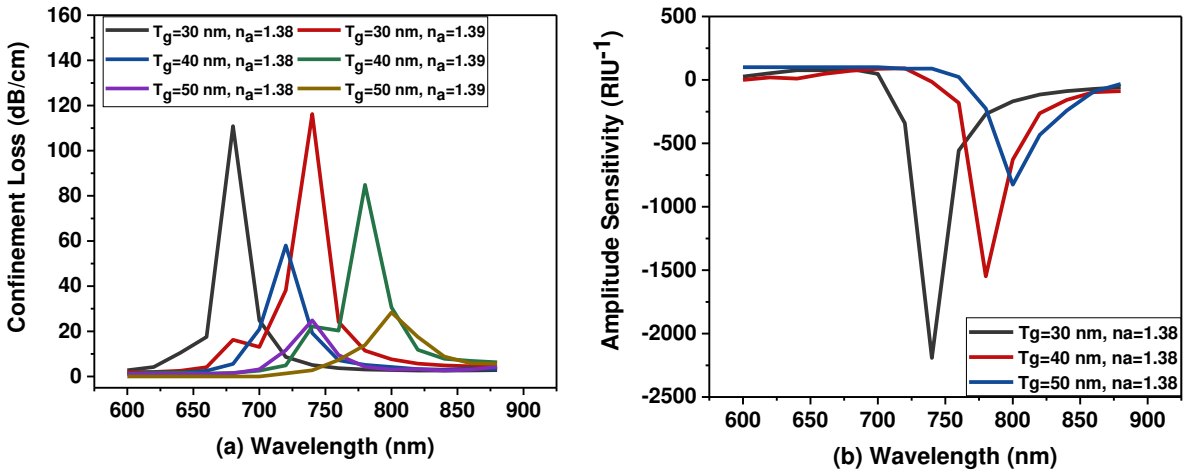

Fig. 6 Effect on the CL peak values due to scaling the gold layer thickness from 30 nm to 50 nm and (b) variation of amplitude sensitivity for ARI 1.38

3.3 Sensor performance analysis on the effect of lattice period

In this sub-section, the effect of lattice period Λ on the confinement loss and corresponding amplitude sensitivity has been simulated and plotted in Fig. 7(a) and (b), respectively. Variation in CL spectrum is plotted with the different values of Λ 1.7 µm, 1.75 µm, and 1.8 µm. Minimum and maximum loss peaks vary over the wavelength range from 660 nm to 780 nm. Peak resonance wavelength shifted towards a lower wavelength while increasing the lattice period from 1.7 µm to 1.8 µm. The calculated amplitude sensitivity variation has been displayed in Fig. 7(b). For Λ = 1.7 µm observed AS is 1652 RIU^{-1}, for Λ= 1.75 µm AS is as 2191 RIU^{-1}, and for Λ=1.8 µm AS is as 1342 $RIU^{-1}$for the analyte RI of 1.38. Therefore, from Fig. 7(b), the highest sensitivity is achieved with the lattice period of 1.75 µm.

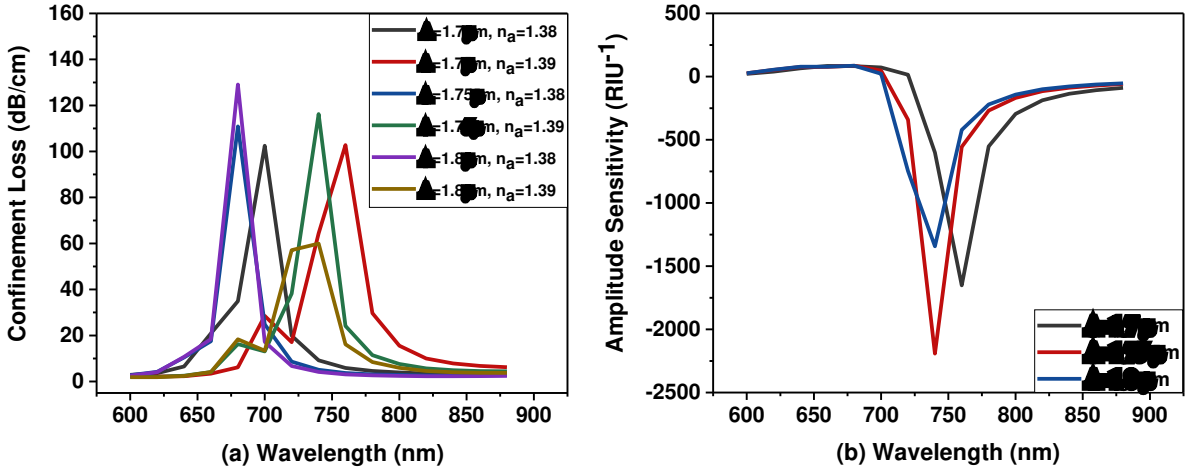

Fig. 7 Dependence of CL spectrum (b) Amplitude sensitivity variation when lattice period is varied from 1.7 µm to 1.8 µm over the ARI of 1.38 and 1.39

3.4 Sensor performance analysis on the effect of small air hole diameter

The result of varying the diameter of small air hole d_s on the sensor sensitivity has been analyzed. CL spectra and corresponding amplitude sensitivity graphs for different values of d_s are demonstrated in Fig. 8(a) and (b), respectively. CL peak increases from 83 to 118 dB/cm when d_s is 0.3 µm. Peak shifts from 117 to 230 dB/cm when d_s is 0.4 µm, and 168 to 106 dB/cm when d_s is 0.5 µm. These loss values are observed for ARI variation from 1.39 to 1.40. According to these observed CL values, amplitude sensitivity values are1546, 3959, and 2708 RIU^{-1} for different values of d_s 0.3, 0.4 and 0.5 µm respectively, at ARI of 1.39. As per the simulated results, d_s value of 0.4 µm is selected for the analysis of sensor behavior. Beyond this d_s value (upward or downward), amplitude sensitivity decreases due to reduction in mutual coupling efficiency as depicted in Fig. 8(b).[30]

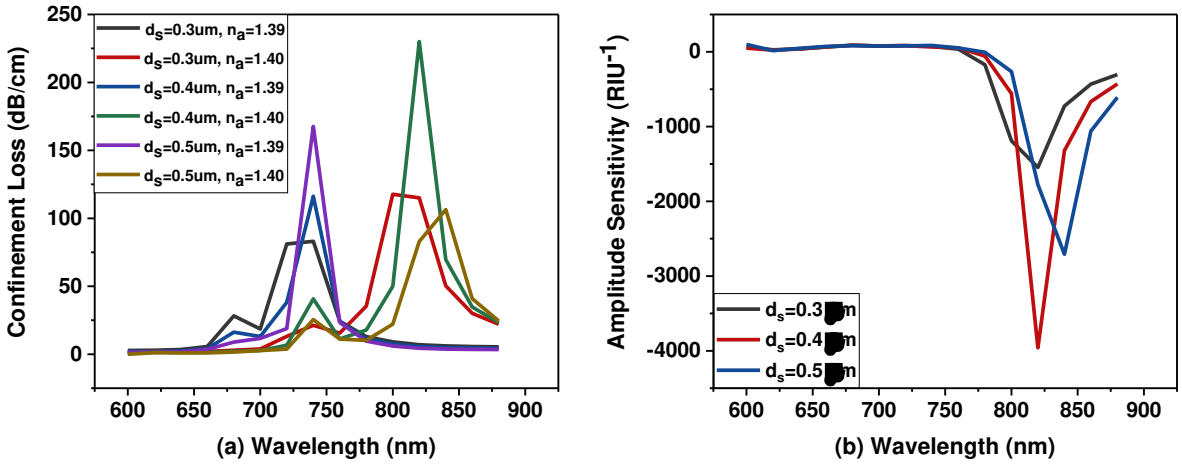

Fig. 8 Variation in (a) CL spectra, and (b) amplitude sensitivity with variation in small air hole diameters from 0.3 µm to 0.5 µm at ARI values of 1.39 and 1.40

Polynomial fit is an important factor in analyzing the sensor performance. This relation is obtained between peak resonance wavelength and respective analyte RI as shown in Fig. 9. Here, ARI is taken on the horizontal axis and dependent variable resonance wavelength is taken on the vertical axis. Polynomial fitting equation with R-value is shown in the inset of Fig.9. Because of good polynomial fit proposed sensor offers high sensitivity for ARI detection.[20]

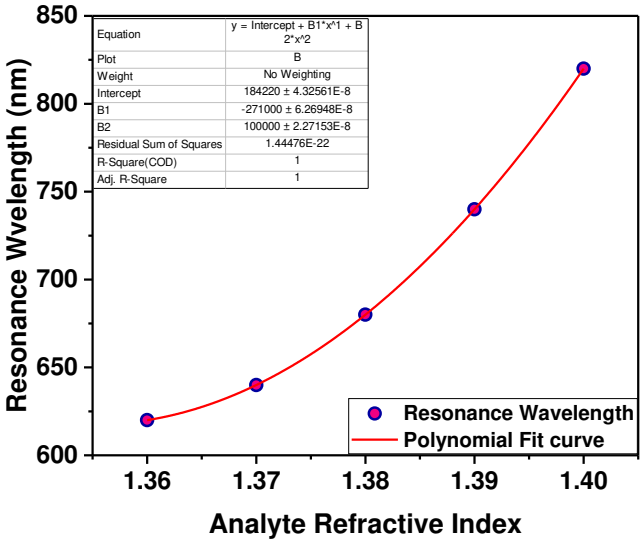

Fig. 9 Polynomial fit response of the investigated PCF-SPR sensor

A comparison has been evaluated between published PCF-SPR sensor and suggested PCF-SPR sensor as a final interpretation of the investigated sensor in Table 1.The suggested sensor design offers enhanced simulated results in terms of sensor detection ability.

Table 1

Comparison between existing SPR-PCF sensor and reported SPR-PCF sensor

Ref.	Sensor design	Wavelength Sensitivity	Amplitude Sensitivity	Analyte RI
[22]	Dual-core PCF-SPR sensor	8000nm/RIU	700 RIU^{-1}	1.45-1.48
[23]	Solid-core PCF-SPR sensor	4000 nm/RIU	478 RIU^{-1}	1.33-1.37
[24]	Open-channel PCF-SPR sensor	5000nm/RIU	396 RIU^{-1}	1.33-1.39
[25]	Circular PCF-SPR sensor	9000 nm/RIU	318 RIU^{-1}	1.34-1.37
[26]	Spiral PCF-SPR sensor	4300 nm/RIU	420.4 RIU^{-1}	1.33 -1.38
	Proposed PCF-SPR sensor	**8000 nm/RIU**	**3959 RIU^{-1}**	**1.36-1.40**

Conclusion

A regular hexagonal solid core SPR based PCF sensor is proposed and analyzed in terms of sensitivity performance. The deposition of less oxidized gold plasmonic material surrounding the PCF geometry offers a compact structure for manufacturing and enhances the recognition process. Structure parameters such as gold layer thickness, lattice period, and air hole diameters are optimized to detect the ARI range from 1.36 to 1.40. Simulated results present a high wavelength sensitivity of 8000 nm/RIU and a high value of amplitude sensitivity of 3959 RIU^{-1}. Obtained results make it competent for recognizing biological elements, chemical and liquids samples.[32-34]

Declarations

Funding Not applicable

Conflicts of interest No

Availability of data and material Not applicable

Code availability Not applicable

Authors' contribution Co-author guided me to complete this research work

References

[1] S. Yin, "Fiber Optic Sensors", Taylor & Francis Group, 2nd Ed. (2008).

[2] Ademgil, Huseyin. "Highly sensitive octagonal photonic crystal fiber based sensor," Optik-Inter Jour. for Light and Electron Optics.125(20), 6274-6278 (2014)

[3] A. Rifat, R. Ahmed, A. K. Yetisen, H. Butt, A. Sabouri, G. A. Mahdiraji, S. H. Yun, and F. M. Adikan, "Photonic crystal fiber based plasmonic sensors," Sens. Actuators B Chem. 243, 311–325 (2017).

[4] Asaduzzaman, S., Ahmed, K., Bhuiyan, T. and Farah, T., "Hybrid photonic crystal fiber in chemical sensing," Springer Plus, 5(1) 748 (2016).

[5] R. W. Wood, "XLII. On a remarkable case of uneven distribution of light in a diffraction grating spectrum" Lond. Edinb. Dublin. Philos. Mag. J. Sci. 4(21), 396–402 (1902)

[6] R. C. Jorgenson, and S. S. Yee, "A fiber-optic chemical sensor based on surface plasmon resonance" Sens. Actuators B Chem. 12(3), 213–220 (1993)

[7] J. Homola, "Present and future of surface plasmon resonance biosensors" Anal. Bioanal. Chem. 377, 528–539 (2003)

[8] C. Mouvet, R. D. Harris, C. Maciag, B. J. Luf, J. S. Wilkinson, J. Piehler, A. Brecht, G. Gauglitz, R. Abuknesha, and G. Ismail, "Determination of simazine in water samples by waveguide surface plasmon resonance" Anal. Chim. Acta 338(1–2), 109–117 (1997)

[9] Y. –C. Cheng, S. Wen-Kuan, and J.-H. Liou, "Application of a liquid sensor based on surface plasma wave excitation to distinguish methyl alcohol from ethyl alcohol" Opt. Eng. 39(1), 311–314 (2000)

[10] H. Thenmozhia , M.S. Mani Rajana, and K. Ahmed, "D-shaped PCF sensor based on SPR for the detection of carcinogenic agents in food and cosmetics" Optik, 180, 264-270 (2019).

[11] V. Kaur, and S. Singh, "Design approach of solid-core photonic crystal fiber sensor with sensing ring for blood component detection," J. Nanophoton. 13(2), 026011 (2019).

[12] V. Kaur and S. Singh, “A dual-channel surface plasmon resonance biosensor based on a photonic crystal fiber for multianalyte sensing,” J. Comput. Electron. 18(1), 319–328 (2019).
[13] H. Chopra, R. S. Kaler, and B. Painam, “Photonic crystal waveguide-based biosensor for detection of diseases,” J. Nanophotonics 10(3), 036011 (2016).
[14] M. Morshed, M. I. Hasan, and S. M. A. Razzak, “Enhancement of the sensitivity of gas sensor based on microstructure optical fiber,” Photonic Sens. 5(4), 312–320 (2015).
[15] V. Kaur and S. Singh, “Design of titanium nitride coated PCF-SPR sensor for liquid sensing applications,” Opt. Fiber Technol. 48, 159–164 (2019).
[16] U. S. Dinish et al., “Highly sensitive SERS detection of cancer proteins in low sample volume using hollow core photonic crystal fiber,” Biosens. Bioelectron. 33(1), 293–298 (2012).
[17] P. Sharma and P. Sharan, “Design of photonic crystal based ring resonator for detection of different blood constituents,” Opt. Commun. 348, 19–23 (2015).
[18] M. R. Momota and M. R. Hasan, “Hollow-core silver coated photonic crystal fiber plasmonic sensor,” Opt. Mater. 76, 287–294 (2018).
[19] Md. B. Hossain, S.M. R. Islam, K.M. T. Hossain , L. F. Abdulrazak , Md. N. Sakib, I.S. Amiri, “High sensitivity hollow core circular shaped PCF surface plasmonic biosensor employing silver coat: A numerical design and analysis with external sensing approach” Results in Physics 16, 102909 (2020).
[20] Md. N. Sakib, S.M. R. Islam, T.V. Mahendiran , L. F. Abdulrazakd, Md. S. Islam, I. M. Mehedi, Q.M. Kamrunnahar, M. Momtaj, Md. W. Hassan, I.S. Amiri, Md. B. Hossain, “Numerical Study of Circularly Slotted Highly Sensitive Plasmonic Biosensor: A Novel Approach” Results in Physics 17, 103130 (2020).
[21] Md. N. Sakib, Mb. B. Hossain, K. F. Al-tabatabaie , I. M. Mehedid , Md. T. Hasan , Md. A.Hossain , and I.S. Amiri, “High performance dual core D-shape PCF-SPR sensor modeling employing gold coat” Results in Physics 15, 102788 (2019).
[22] A. Shafkat, “Analysis of a gold coated plasmonic sensor based on a duplex core photonic crystal fiber” Sensing and Bio-Sensing Research 28 (2020) 100324
[23] A. A. Rifat, Md. R. Hasan, R. Ahmed, and H. Butt, “Photonic crystal fiber-based plasmonic biosensor with external sensing approach” ” J. Nanophoton. 12(1), 012503 (2017),
[24] S. Akter, Md. Z. Rahman, and S. Mahmud, “Highly sensitive open-channels based plasmonic biosensor in visible to near infrared wavelength” Results in Physics 13, 102328 (2019).
[25] S. Chakma, M.A. Khalek, B.K. Paul, K. Ahmed, M.R. Hasan, A.N. Bahar, Gold-coated photonic crystal fiber biosensor based on surface plasmon resonance: design and analysis. Sens. BioSens. Res. 18, 7–12 (2018)
[26] Md. R. Hasan, S. Akter, A. A. Rifat, S. Rana, K. Ahmed, R. Ahmed, H. Subbaraman, and D. Abbott, “Spiral Photonic Crystal Fiber-Based Dual-Polarized Surface Plasmon Resonance Biosensor” IEEE Sensors Journal 18(1), (2018).
[27] M.R. Hasan, S. Akter, A.A. Rifat, S. Rana, and S. Ali, “A highly sensitive gold-coated photonic crystal fiber biosensor based on surface plasmon resonance” Photonics 4(1), 18 (2017).
[28] C. Liu, L. Yang, W. Su, F. Wang, T. Sun, Q. Liu, H. Mu, and P.K. Chu, “Numerical analysis of a photonic crystal fiber based on a surface plasmon resonance sensor with an annular analyte channel” Opt. Commun. 382, 162–166 (2017).
[29] N. A. E. Issa, M. A. Eijkelenborg, M. Fellew, F. Cox, G. Henry, and M. C. Large, “Fabrication and study of micro structured optical fibers with elliptical holes” Opt. Lett. 29, 1336–1338 (2004).
[30] A. A. Rifat, R. Ahmed, A. K. Yetisen, H. Butt, A. Sabouri, G. A. Mahdiraji, S. H. Yun, and F. M. Adikan, “Photonic crystal fiber based plasmonic sensors,” Sens. Actuators B Chem. 243, 311–325 (2017).
[31] A. A. Rifat, R. Ahmed, G. A. Mahdiraji, F. M. Adikan, and A. E. Miroshnichenko, “Highly sensitive selectively coated photonic crystal fiber-based plasmonic sensor,” Opt. Lett. 43, 891–894 (2018).
[32] Y. Zhao, Z.-Q. Deng, and J. Li, “Photonic crystal fiber based surface plasmon resonance chemical sensors,” Sens. Actuators B Chem. 202, 557–567 (2014).
[33] X. Chen, L. Xia, and C. Li, “Surface plasmon resonance sensor based on a novel D-shaped photonic crystal fiber for low refractive index detection,” IEEE Photon. J. 10, 6800709 (2018).

[34] M. Liu, X. Yang, P. Shum, and H. Yuan, “High-sensitivity birefringent and single-layer coating photonic crystal fiber biosensor based on surface plasmon resonance,” Appl. Opt. 57, 1883–1886 (2018).

Figures

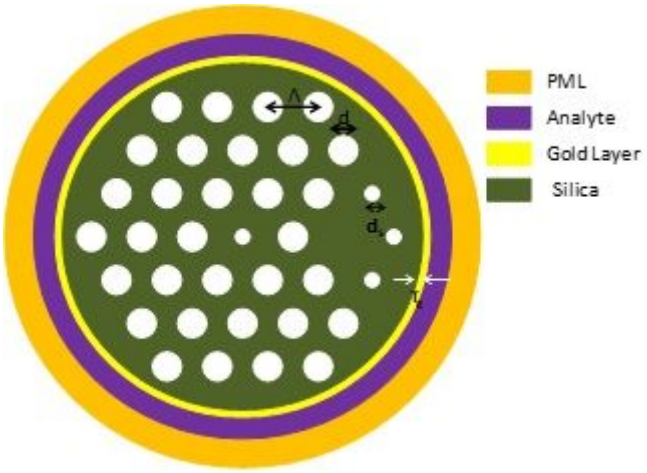

Figure 1

transverse image of SPR-PCF sensor

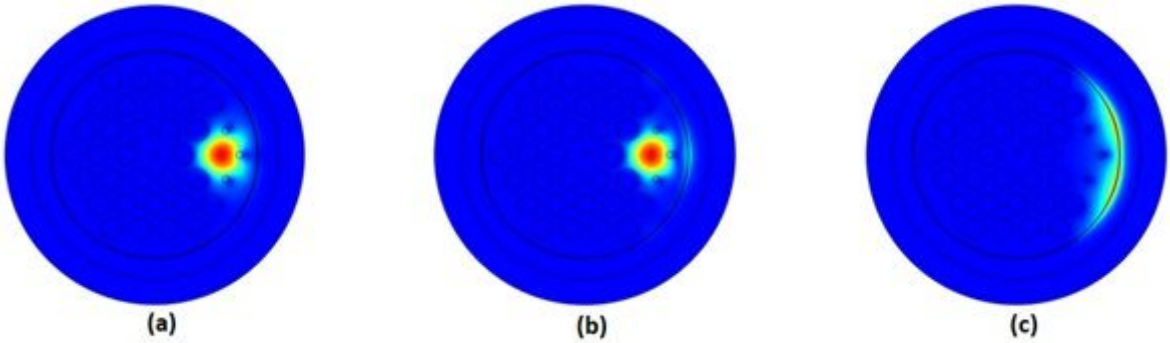

Figure 2

Power distribution mode (a) X-polarized mode (b) Resonance mode (c) Surface Plasmon mode

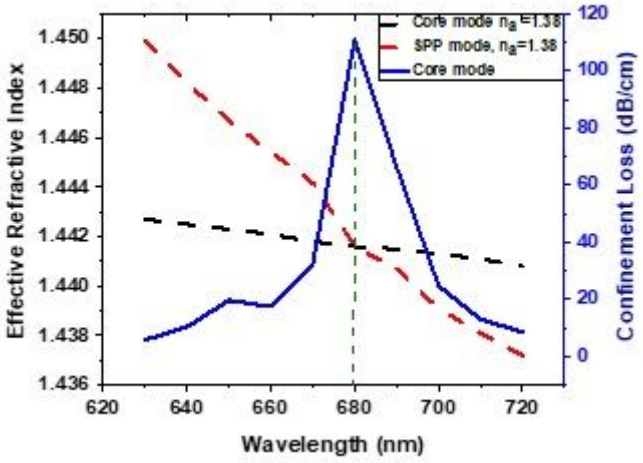

Figure 3

Intersection of Core and SPP mode with core confinement loss curve

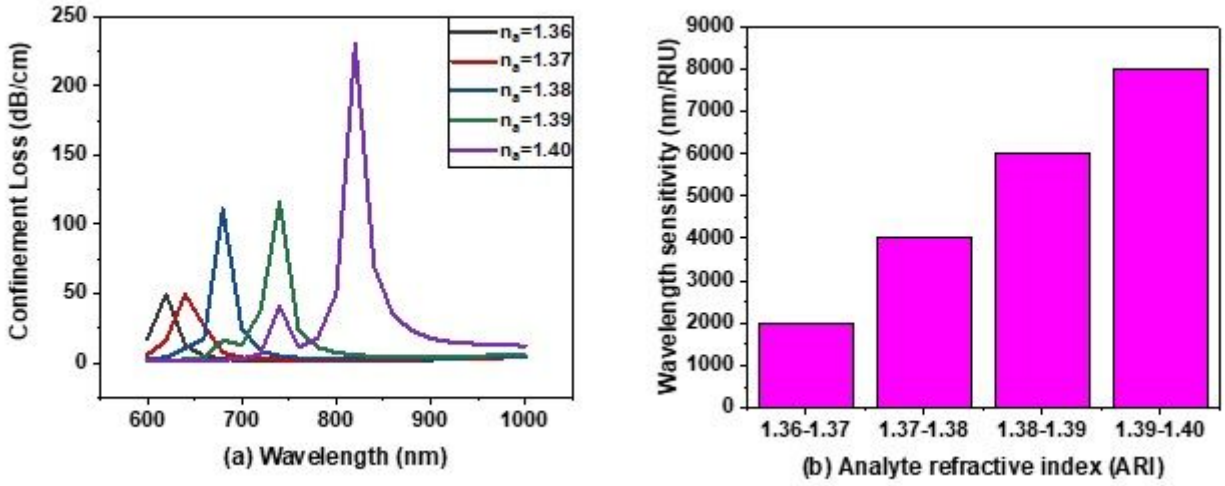

Figure 4

Simulated curves of confinement loss when =1.75 μm, d= 1.2, =0.4 μm, and Tg=30 nm for different values of ARI from 1.36 to 1.40 (b) Wavelength sensitivity chart for different ARI

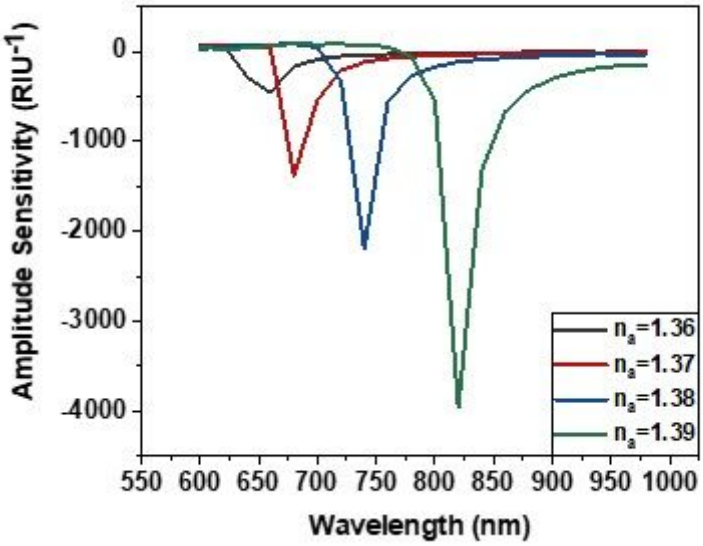

Figure 5

Dependence of amplitude sensitivity according to the range of ARI from 1.36 to 1.39

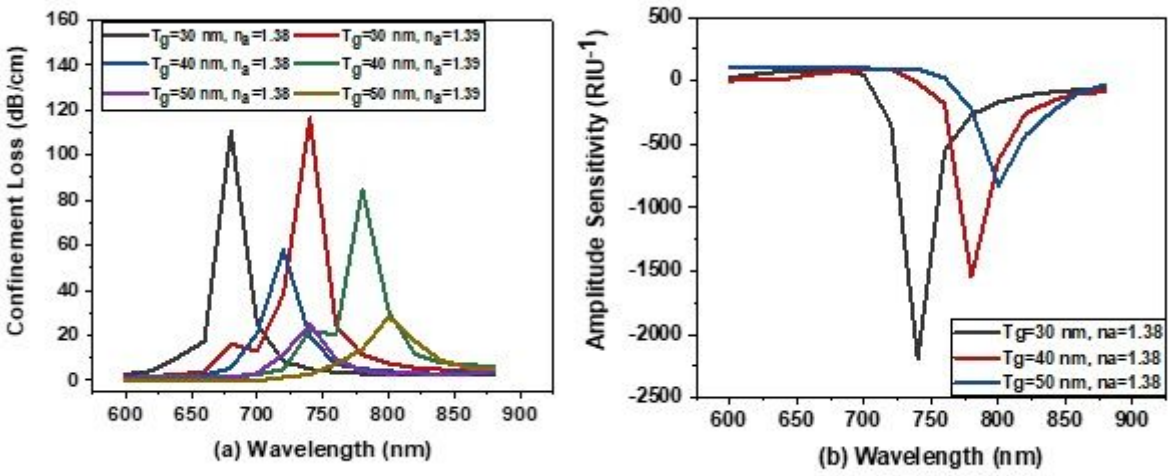

Figure 6

Effect on the CL peak values due to scaling the gold layer thickness from 30 nm to 50 nm and (b) variation of amplitude sensitivity for ARI 1.38

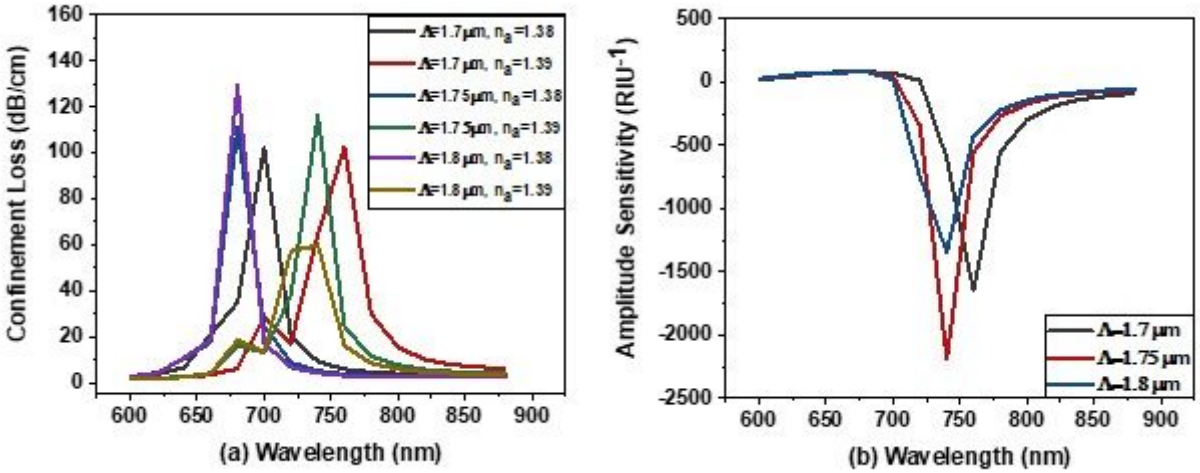

Figure 7

Dependence of CL spectrum (b) Amplitude sensitivity variation when lattice period is varied from 1.7 μm to 1.8 μm over the ARI of 1.38 and 1.39

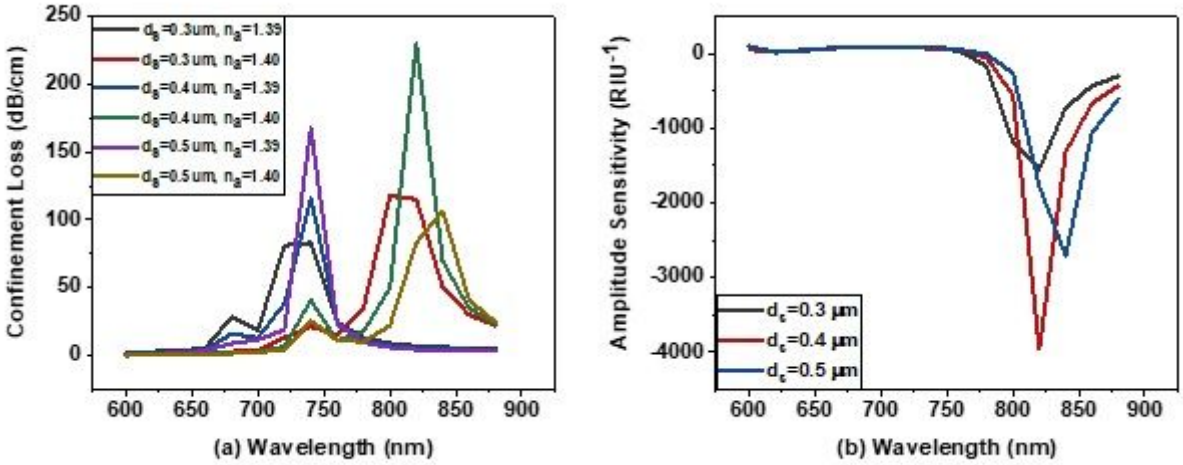

Figure 8

Variation in (a) CL spectra, and (b) amplitude sensitivity with variation in small air hole diameters from 0.3 µm to 0.5 µm at ARI values of 1.39 and 1.40

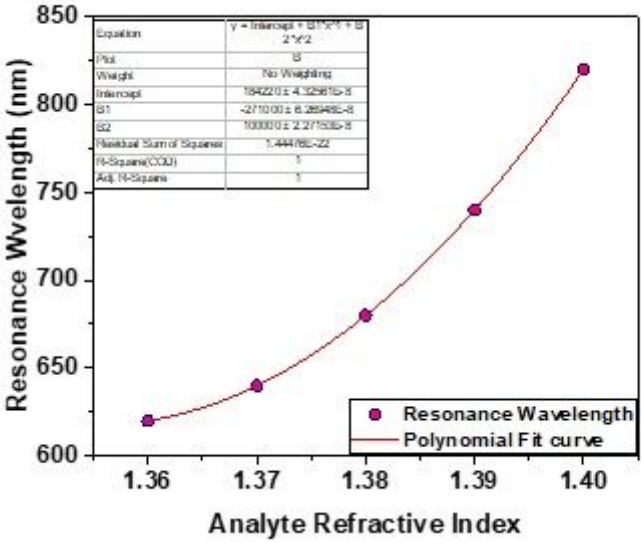

Figure 9

Polynomial fit response of the investigated PCF-SPR sensor